optica

Single-shot multispectral imaging with a monochromatic camera: supplementary material

SUJIT KUMAR SAHOO,[1,2,*] DONGLIANG TANG,[1] AND CUONG DANG[1,*]

[1]Centre for OptoElectronics and Biophotonics (OPTIMUS), School of Electrical and Electronic Engineering, The Photonic Institute (TPI), Nanyang Technological University Singapore, 50 Nanyang Avenue, 639798, Singapore

[2] Department of Statistics and Applied Probability, National University of Singapore, Singapore

*Corresponding author: sujit@pmail.ntu.edu.sg, hcdang@ntu.edu.sg

Published 4 October 2017

This document provides supplementary information to "Single-shot multispectral imaging with a monochromatic camera," https:doi.org/10.1364/optica.4.001209. It contains detailed information regarding the optical setup and the post-processing for the data, measurements for the field of view, demonstrations for mixed color components and a demonstration for the spectroscopy technique with scattering media. In addition, we analyze how the possible factors, such as the number of pixels, spectral bands, accuracy of point spreading function and noises affect the reconstructions.

https://doi.org/10.6084/m9.figshare.5388109

1. Detailed derivation of the principle

Within the memory effect region of a scattering medium, the PSF is linear and shift-invariant. Therefore, the captured speckle pattern I_λ after the scattering medium is the convolution (denoted as $*$) of an object with the optical system. It is expressed as follows:

$$I_\lambda = O_\lambda * PSF_\lambda$$

Convolution in spatial domain becomes the multiplication in Fourier domain:

$$FFT(O_\lambda * PSF_\lambda) = FFT(O_\lambda)FFT(PSF_\lambda)$$

Thus, the object O_λ can be recovered from its speckle pattern I_λ by deconvolution: $O_\lambda = deconv(I_\lambda, PSF_\lambda)$, if we know the PSF at wavelength λ. It is ideally expressed as follows:

$$deconv(I_\lambda, PSF_\lambda) = FFT^{-1}\left(\frac{FFT(I_\lambda)FFT(PSF_\lambda)^c}{\left|FFT(PSF_\lambda)\right|^2}\right), \quad \textbf{(S1)}$$

where $(.)^c$ is the complex conjugate, $FFT(.)$ and $FFT^{-1}(.)$ are the Fourier transform and its inverse, respectively. As a result of spectral decorrelation in strongly scattering media, the speckle patterns are wavelength dependent; and spectrally separated light sources produce uncorrelated speckle patterns. Using this spectrum dependent behavior of strongly scattering media, spectrometers with high spectral resolution have been demonstrated [1-4]. This spectral decorrelation can be mathematically expressed as follows.

$$PSF_{\lambda 1} \star PSF_{\lambda 2} \approx \begin{cases} 0 & if \quad \lambda 1 \neq \lambda 2 \\ \delta & if \quad \lambda 1 = \lambda 2 \end{cases}, \quad \textbf{(S2)}$$

where $\star$ is the correlation operator, and δ is the spatial impulse function. And the speckle pattern of the multispectral object is a composite response of the scattering medium with all the wavelengths in the object's spectral bandwidth, which can be expressed as follows:

$$I = \sum_\lambda I_\lambda = \sum_\lambda (O_\lambda * PSF_\lambda)$$

Let's derive the following equality

$$\begin{aligned} & \sum_{\lambda \neq \lambda 1} FFT(I_\lambda)FFT(PSF_{\lambda 1})^c \\ = & \sum_{\lambda \neq \lambda 1} FFT(O_\lambda)FFT(PSF_\lambda)FFT(PSF_{\lambda 1})^c \\ = & \sum_{\lambda \neq \lambda 1} FFT(O_\lambda)FFT(PSF_\lambda \star PSF_{\lambda 1}) \end{aligned}$$

Now, using spectral decorrelation property of equation (S2), it can be stated as follows:

$$\sum_{\lambda \neq \lambda 1} FFT(I_\lambda) FFT(PSF_{\lambda 1})^c \approx 0 \qquad \textbf{(S3)}$$

Using the above equality we can state that

$$\begin{aligned} & FFT(I) FFT(PSF_{\lambda 1})^c \\ = \; & FFT(I_{\lambda 1}) FFT(PSF_{\lambda 1})^c + \sum_{\lambda \neq \lambda 1} FFT(I_\lambda) FFT(PSF_{\lambda 1})^c \\ \approx \; & FFT(I_{\lambda 1}) FFT(PSF_{\lambda 1})^c \end{aligned}$$

From the deconvolution expression in equation (S1), we arrive to the following conclusion.

$$\begin{aligned} & FFT(I) FFT(PSF_{\lambda 1})^c \approx FFT(I_{\lambda 1}) FFT(PSF_{\lambda 1})^c \\ \Rightarrow \; & deconv(I, PSF_{\lambda 1})^c \approx deconv(I_{\lambda 1}, PSF_{\lambda 1})^c \end{aligned}$$

Therefore, each spectral band of the object can be reconstructed from a single monochromatic image I as follow.

$$O_\lambda \approx deconv(I, PSF_\lambda) \qquad \textbf{(S4)}$$

It is worth to note that the single wavelength λ presented in this principle can be extended to be a spectral band, and different values of λ present different disjointed bands.

2. Optical setup and data processing

A common projector (Acer X113PH) without the second projection lens is utilized to generate 2D multispectral objects at the plane of iris-1 [Fig. 2(a)]. The small lens inside the projector makes the magnification of $M_1 \approx 1.82$ from its DMD chip to the object plane. The diffuser (Edmund, 120 Grit Ground Glass Diffuser) combined with the iris-2 are positioned at a distance $u \approx 210mm$ from the object plane. The diameter of the iris-2 is about 2mm to obtain an appropriate speckle intensity and signal-to-noise ratio. The speckle patterns measured by the camera is the integration of the speckle patterns produced by all the illuminated area of the diffuser. A larger area of diffuser yields a poor contrast speckles, which is difficult to resolve in limited dynamic range. Therefore, Iris 2 is used to control the exposed area of the diffuser that helps in reducing the speckle contrast [5]. The light coming from the 2D object passes through the diffuser and generates the speckle pattern on a 16-bit monochromatic CMOS (Andor Neo 5.5, 2560×2160, pixel size 6.5um), which is placed at a distance $v \approx 87.5mm$ from the diffuser. Therefore, the magnification of our imaging setup is $M_2 = v/u \approx 0.42$ and the total magnification from the DMD chip to CMOS sensor is $M_{total} = M_1 \cdot M_2$. The pixel size of the camera should be small enough to sample the speckle correctly according to Nyquist theorem. The resolution depends on the Numerical Aperture (N.A.) of the system as it defines spatial frequency cut-off of our imaging system. The N.A. can be controlled by adjusting the iris 2 aperture and spacing between the object and diffuser. We apply the Wiener deconvolution algorithm, which takes about 0.5 second for each spectral image to be reconstructed, using MATLAB on a normal PC (Intel Core i7, 16 GB memory). Spectral PSFs are constant for an optical system and their FFT can be pre-calculated and stored to reduce the reconstruction process by 30% (Visualization 1). The central area with 2048*2048 pixels on the CMOS sensor is chosen for our experiments. All the speckle images and PSFs are grey images as they are captured by a monochromatic camera. We set colours into these multispectral PSFs and multispectral images for our illustration purpose only.

For each speckle patterns and PSFs, we divide them with their low frequency envelop to remove the hallow effect and sharpen the speckles. The superimposed images are created from spectral images with our defined colours for the illustration purpose as well. All the superimposed images (colour images) are composite of 3 reconstructed red, green and blue (RGB) spectral images without any colour processing. The spectra of white, and RGB light from the projector are measured by Avantes spectrometer (AvaSpec-2048).

3. Measurement for the field of view (FOV)

Any object located in the memory effect region of the scattering medium generates the shift-invariant speckle pattern on the camera. This memory effect region is the incident angle region (ϕ), defining the field of view (FOV) in our experiment: $F = \phi u$, where u is the distance from object plane (iris-1's plane) to the scattering medium. The "ON" pixels on the digital micro-mirror device (DMD) of projector define the 2D object on the object plane with magnification of $M = 1.82$. We characterize the FOV by measuring the cross-correlation coefficient between the PSF at the centre and PSFs at different positions (x). Figure S1 presents the PSF cross-correlation coefficient as a function of point's position on the object plane. If we define the FOV is the region with PSF cross-correlation coefficient of greater than 0.5, the FOV will be inside the circle with diameter of about 3.2 mm. We also can estimate the effective thickness of scattering medium (L) by fitting the experiment data with the theoretical model for the memory effect as follows [6]:

$$C(\theta, L) = [k_0 \theta L / \sinh(k_0 \theta L)]^2 \qquad \textbf{(S5)}$$

where C is the correlation coefficient, k_0 is the wave vector ($k_0 = 2\pi/\lambda$), and $\theta = x/u$ is the incident angle. If we use light at wavelength (λ) of peak intensity which has the main contribution in creating a PSF to calculate k_0 , we can estimate roughly the effective thickness of our scattering medium of about: 18, 22, 18 and 16 μm for white and RGB band, respectively. Object extending beyond the field of view (FOV) causes loss of speckle contrast by adding unwanted speckle patterns. As we want to preserve the speckle contrast in the given dynamic range of the system, we should operate within the FOV of the system. This helps us devote the dynamic range of the system in resolving the speckle patterns of the multispectral object. However, if we can have ultra-high dynamic range camera, the larger object would not be a problem. The object beyond the FOV would automatically be filtered out during the deconvolution process, and the object within the field of view would be reconstructed alone [7].

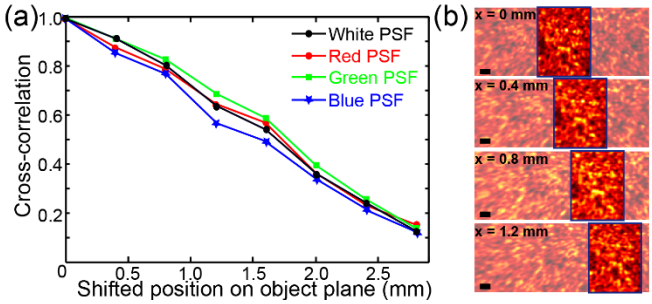

Fig. S1. Memory effect in our strongly scattering medium. (a) Cross-correlation coefficient between the PSF at the centre (x = 0) and PSFs at other positions. The experiment is repeated for four spectral bands: RGB and white. (b) Selected region of white PSFs at different positions. Highlighted regions show the shift-invariant speckle patterns when the

white colour pixel at the positions of x = 0, 0.4, 0.8, 1.2 mm, respectively. Scale bars: 100μm.

4. Effect of spectral overlap on the reconstructed multispectral images

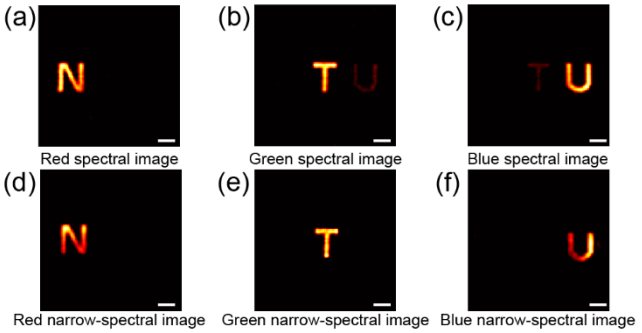

Fig. S2. Effects of spectral overlap in PSFs, presented in heat-map images. (a-c) The RGB spectral images, respectively, i.e. the heat-map version of Fig. 2(d) for RGB images only. The cross-talk effect is observed between green and blue spectral channels due to their spectral overlap. (d-f) The RGB narrow-spectral band images, i.e. the heat-map version of Fig. 3(c), respectively. Non-overlap in spectra of these RGB narrow-spectral PSFs [Fig. 3(d)] makes separated N, T, U letters in three RGB spectral images. However, the weak intensities of a single projector's pixel with narrow band filters in green and especially blue region make pure measurements (very low SNR) of narrow-spectral PSFs. This low SNR reduces the quality of reconstructed spectral images in narrow green (e) and especially narrow blue (f) band. Scale bars: 100 μm.

5. Demonstrations for mixed color components.

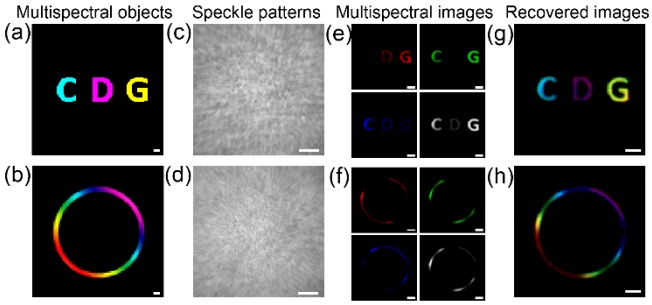

Fig. S3. Reconstruction of mixed and gradient multispectral objects. (a) Multispectral 'CDG' letters with corresponding cyan, magenta and yellow (CMY) colour are generated as an object. In display technology, CMY colours are generated by combination of three primary RGB colours: cyan is a mixture of green and blue, magenta is a mixture of red and blue, yellow is a mixture of red and green. (b) Another object of a circular ring with gradient rainbow colours. (c), (d) The raw speckle patterns captured by the monochromatic camera for the object in (a) and (b), respectively. (e), (f) Reconstructed spectral images from the raw speckle images in (c) and (d), respectively. We use the corresponding spectral PSFs in Figure 2(c) for the deconvolution processes. (g), (h) The composite spectral image of the object is created by super positioning three RGB spectral images from (e) and (f), respectively. Scale bars: 1000 μm in (c) and (d); 100 μm in others.

We further demonstrate our technique with more complex spectral information in Fig. S3. Three letters CDG [Fig. S3(a)] presented in cyan (green and blue), magenta (red and blue), and yellow (red and green), respectively or a complex multispectral object with gradient and blended colours [Fig. S3(b)] are utilized to highlight the capabilities of our technique. Four spectral PSFs as used for recovering in Fig. 2(c) are employed to de-convolve the raw speckle images in Fig. S3(c)-(d). The reconstructed multispectral images in Fig. S3(e) presents successful recovery of the pairs of letters that shares the same spectral element in Fig. S3(a) by the respective RGB spectral PSFs. Deconvolution with the white spectral PSF results in three letter CDG as expected with strong intensity at letters C and G because of the strong green intensity in white spectrum [Fig. 3(b)]. Figure S3(f) shows the recovered multispectral images of object in Fig. S3(b) with gradient intensities. The final composited "rainbow" colour images are displayed in Fig. S3(g)-(h), resembling the original complex multispectral object in Fig. S3(a)-(b), respectively. The colour quality is distorted by the wavelength dependence of camera sensitivity, which is highest at green and lowest at blue range. Calibrating with sensitivities of the camera and human eyes in a colour processing technique as normal colour cameras do will enhance the colour appearance of superimposed images to be similar to the original object.

6. A spectroscopy technique with strongly scattering media

We now demonstrate the ability of our technique to resolve spectral information of a point source. Here, we pass a broadband light point source through the scattering medium, and measured speckle intensities using a monochromatic camera. Then, we construct the spectrum of the broadband point source by calculating the cross-correlation coefficient between the the multispectral PSFs with the measured broadband speckle image. One can use a broadband light source with a monochromator to measure various spectral PSFs at different wavelengths. This one-time "calibration" step could be done at a manufacture. To demonstrate the proof of concept, we numerically simulate various spectral PSFs as independent speckle patterns. The number of spectral PSFs is the product of spectral sampling rate (sample/nm) and the spectral bandwidth. Then, the speckle for a broadband point source is generated by weighted combination of these independent spectral PSFs, where the weights equal to the intensities of the respective spectral lines. We measure the spectrum of a commercial white LED and use it as the broadband for our demonstration. The recovered spectra and the original spectrum is plotted together in Fig. S4. The results show successful recovery of actual spectrum. We simulate here with different spectral sampling rates of $\Delta\lambda$ = 2 nm and 10 nm, in which the PSFs for λ and $\lambda+\Delta\lambda$ are independent, i.e. de-correlated. In reality, how much they are de-correlated and how well our camera detects their differences will define the spectral resolution of our approach. Special design of scattering media can achieve the spectrometer resolution of sub-nanometer [1-4]. For normal optical diffuser or biology tissue, Ori Katz et al. used a tune-able laser to characterize the spectral decorrelation bandwidth of 5 - 10 nm for 20μm-thick sample of TiO_2 particles of diameter <250nm or 500μm-thick chicken breast in their optical setup [5]. For any specific scattering medium, increasing effective thickness will reduce the spectral decorrelation bandwidth, therefore increase the spectral resolution in our spectrometer applications. Nevertheless, the 5~10 nm resolution of the normal diffuser is already useful for many purposes. For example, one can make a simple spectrometer with scattering medium and a smartphone to characterize our LED spectrum.

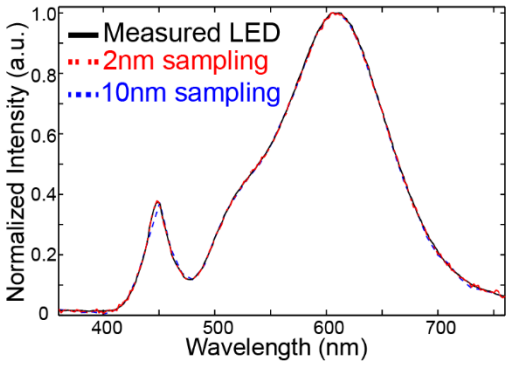

Fig. S4. Demonstration of spectrometer application utilizing spectral decorrelation of PSFs through a scattering medium. Spectrum reconstruction with various separation spectral lines (2 nm and 10 nm, respectively).

7. Deconvolution in presence of noise

The notion of deconvolution has been introduced in the main text and the previous section to have simple illustration of the principle. However, the deconvolution is not just an ideal inversion of the PSF. In the practice, we have to operate in the finite precision and within a fixed dynamic range of the system. In order to handle all these practical constrains, the observed image is mathematically expressed as

$$I = I_{ideal} + V \tag{S6}$$

where $I_{ideal} = \sum_{\lambda} O_{\lambda} * PSF_{\lambda}$, and V is modeled as an additive white Gaussian noise of variance σ^2. Such kind of model can lead us to a very close approximation to the PSF inversion. There exist numerous deconvolution techniques to solve the problem model [8-11]. Weiner deconvolution is one of the fastest technique, which we use throughout our simulations and experiments [8]. The formula for the deconvolution is the following.

$$O_{\lambda} = weiner(I, PSF_{\lambda}) = FFT^{-1}\left(\frac{FFT(I)FFT(PSF_{\lambda})^{C}}{\left|FFT(PSF_{\lambda})\right|^{2} + C\sigma^{2}}\right) \tag{S7}$$

where C>1 is a constant to keep the approximate solution clear from the measurement deformation artifacts. The Weiner deconvolution formula is also very intuitive and it has close resemblance with the ideal deconvolution (Eq. S3). In practice the noise variance of the imaging system/environment can be measured and the value of C can be determined.

There are many existing iterative deconvolution algorithms such as Richardson–Lucy that doesn't need the noise variance parameter [11-13]. However, the noise estimation and reduction is automatically taken care within the iteration loops. As a result, they produced heavily smooth images with other artifacts. The main drawbacks of these iterative algorithms are the execution time that grows in polynomial-scale with total pixels (N) and needs many iteration, whereas Weiner algorithm's execution time is in logarithmic-scale of N without any iterations. The study of various deconvolution methods is beyond the scope of this work, but it might be worth to test our principle with various deconvolution techniques.

8. Effect of imager's resolution (number of pixels)

All the measurement and finite precision noise are always modeled as independent additive noise. However this assumption is only valid in infinite dimension (number of pixels) and infinite precision. As a result, all the convolution algorithms suffer from reconstruction artifacts depending on the amount the correlation between the noise and the signal. In principle, the correlation is a decreasing function [14] of total pixels (N). To demonstrate that we plot the cross-correlation's value of two independent random signals with respect to the number of pixels, taking an average over 1000 trials.

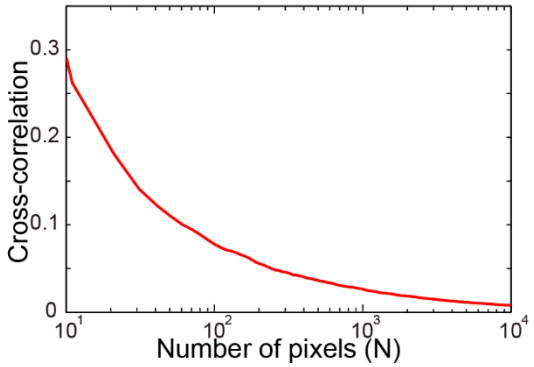

Fig. S5. Cross-correlation coefficient of two independent random images at various number of pixel.

To visually illustrate the effect of the number of pixels on the reconstruction artifacts, we have reconstructed the object by cutting out various size of the measured speckle image and the measured PSFs. We simulate independent speckle patterns for RGB spectral PSFs. Each color component is convolved with the respective PSFs and summed up to form the measured gray scale image. Each of the color component was extracted by deconvolving the speckle image with the respective PSF, and the final image is displayed by superimposing of each reconstructed spectral image in the respective colour channel. The following results are displayed for the various sizes of deconvolution kernels. We can see that the increasing the number of pixels improves quality of the reconstruction image.

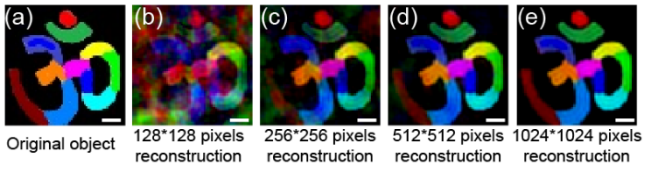

Fig. S6. Effect of the number of pixels in our multispectral imaging technique. (a) An original object of 64x64 pixel. (b-e) The reconstructed multispectral images from the cropped raw speckle image and cropped PSFs at different sizes: 128x128, 256x256, 512x512, 1024x1024, respectively. Scale bars: 10 pixels.

9. Effect of total spectral band numbers

The same notion on increasing correlation can be extended to the principle of multispectral imaging introduced in this letter. The multispectral imaging relies on the spectral decorrelation property of the speckle patterns. This allows us to segregate the superimpose image of each spectral band. The super position can be described as the following.

$$\begin{aligned} I &= O_{\lambda 1} * PSF_{\lambda 1} + \left(\sum_{\lambda \neq \lambda 1} O_{\lambda} * PSF_{\lambda}\right) + V \\ &= O_{\lambda 1} * PSF_{\lambda 1} + (V_{spectra} + V) \end{aligned} \tag{S8}$$

We assumed that the PSF of the recovering bands are uncorrelated to each other (i.e. $PSF_{\lambda 1} \star PSF_{\lambda} \approx 0$, if $\lambda_1 \neq \lambda$). Therefore, the speckle intensity component $V_{spectra} = \sum_{\lambda \neq \lambda 1} O_{\lambda} * PSF_{\lambda}$ is treated as secondary noise. This is very much viable in a larger finite dimension (number of pixels). However, as the number of band increases the component $V_{spectra}$ increases, which will cause

a linear rise in the correlation. As a result, we will have some reconstruction artifacts, which can be suppressed with over-smoothing of the reconstructed images [11].

10. Accuracy of Point Spreading Function

In the previous section, we have discussed the importance of noise, correlation, the number of pixels and number of spectral bands. We have safely assumed the noise only appears during the measurement of the speckle image I. This assumption is quite practical, because the PSF is a one-time measurement. Therefore, more resources such as high-power wavelength tune-able light sources can be devoted to have very accurate spectral PSF measurement at the manufacture. However, our current setup with small projector, the light intensity from a single pixel is very low and our spectral PSFs present some noise. The signal to noise ratio (SNR) is even lower when we use narrow band-pass filters to acquire narrow-spectral PSFs. As a result, we can notice the reconstruction artifacts for some of the bands in our reported results [Fig. S2(f)]. The reconstruction with a noisy PSF can be expressed as follows.

$$O_\lambda = FFT^{-1}\left(\frac{FFT(I)FFT(PSF_\lambda + V_\lambda)^C}{\left|FFT(PSF_\lambda + V_\lambda)\right|^2 + C\sigma^2}\right) \quad \textbf{(S9)}$$

Taking the assumption of the uncorrelated PSF noise V_λ, we can further simplify the expression as follows.

$$O_\lambda \approx FFT^{-1}\left(\frac{FFT(I)FFT(PSF_\lambda)^C}{\left|FFT(PSF_\lambda + V_\lambda)\right|^2 + \left|V_\lambda\right|^2 + C\sigma^2}\right) + [smoothed\ noise] \quad \textbf{(S10)}$$

This deduces that the resulting image would be slightly over smoothed due to $|V_\lambda|^2$, and it would have some smoothed noise due to finite dimension (number of pixels) correlation artifact. A similar imaging experiment as the above section is repeated again for various noise level of the PSF used for reconstruction. The image is generated using the ideal PSFs for convolution, but we have reconstructed the multispectral images with the noisy green PSF. Images are reconstructed for various SNR levels, and the results are displayed in Fig. S7 below. We can observed the degraded reconstruction with the increase in PSF noise.

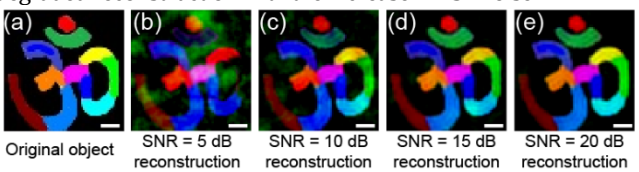

Fig. S7. Effect of noise in PSF measurement on reconstructed multispectral images. (a) An original object of 64x64 pixel. (b-e) The reconstructed multispectral images when the green PSF is corrupted by noise at different SNR level: 5dB, 10dB, 15dB, and 20dB, respectively. Scale bars: 10 pixels.

11. Multispectral imaging of fluorescent sample

The complete experimental setup for a real object decorated with multi-colour fluorescent materials, i.e. colloidal quantum dots (QDs), and experimental data are schematically presented in Fig. S8. The object is lithography mask on glass with opening of 3 letters NTU on which two different quantum dots are decorated. The QD luminescent spectra are presented in Fig. S8 (b) which shows two quantum dots radiate good red and green light without spectral overlap. A tilted light beam from a blue laser (CPS450, wavelength: 450nm) focus into QDs. After propagating through a long-pass edge filter (BLP01-473R-25), a diffuser (Edmund, 120 Grit Ground Glass Diffuser) and an iris, a mixed spectral scattering pattern is recorded on the monochromatic camera (Andor Neo 5.5, 2560×2160, pixel size 6.5um). The distances of *u* and *v* are about 240 mm and 65 mm respectively, then the magnification between the image and object plane is about 0.27. For the green and red PSF measurements, two pinholes with diameter about 90 μm emitting red and green colours from two QDs are presented at the object plane and corresponding speckle patterns as the spectral PSFs are captured on the camera and recorded for the post-processing algorithm. Then a colorful 'NTU' sample with size of about 1.47mm*0.38mm is placed at the position of the pinholes and acted as a real colorful object, as the inset presented in Fig. S8 (a). Figure S8 (d) shows the recovered spectral image by deconvolving the speckle pattern with corresponding spectral PSFs in Fig. S8 (c). Each spectral PSF successfully reconstructs the correct spectral part of object. A composition of these two individual red and green patterns is also presented as a good spectral reconstruction in comparison with the fluorescent microscopy image.

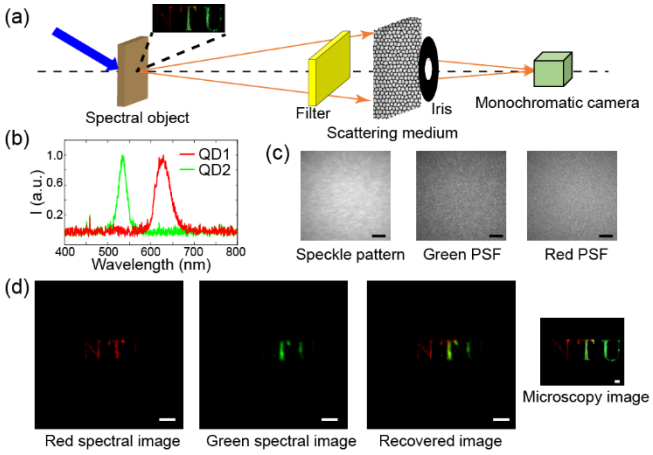

Fig. S8. Multispectral imaging of fluorescent samples (QDs sample). (a) Tilted light beam from a blue laser focus on a 'NTU' sample with two labelling QDs. (b) Fluorescent spectra from two QDs. (c) Measured speckle pattern on the camera from colorful 'NTU' sample and the corresponding PSFs as two pinholes respectively labeled these QDs are placed at the object plane. (d) Reconstructed spectral images with red and green PSF, a composite multispectral image reconstructed by our technique and a fluorescent microscopy image as reference, respectively. Scale bars: 1000 μm in (c) and 100 μm in (d).

References

1. B. Redding, S. F. Liew, R. Sarma, and H. Cao, "Compact spectrometer based on a disordered photonic chip," Nature Photonics **7**, 746-751, (2013).

2. M. Chakrabar'ti, M. L. Jakobsen, and S. G. Hanson, "Speckle-based spectrometer, " Optics Letters **40**, 3264-3267 (2015).

3. M. Mazilu, T. Vettenburg, A. Di Falco, and K. Dholakia, "Random super-prism wavelength meter," Optics Letters **39**, 96-99 (2014).

4. R. French, S. Gigan, and O. L. Muskens, "Speckle-based hyperspectral imaging combining multiple scattering and compressive sensing in nanowire mats," Optics Letters **42**, 1820-1823 (2017).

5. O. Katz, P. Heidmann, M. Fink, and S. Gigan, "Non-invasive single-shot imagingthrough scattering layers and around corners via speckle correlations," Nature Photonics **8**, 784-790 (2014).

6. J. Bertolotti, E. G. van Putten, C. Blum, A. Lagendijk, W. L. Vos, and A. P. Mosk, "Non-invasive imaging through opaque scattering layers," Nature **491**, 232-234 (2012).

7. Edrei, E. & Scarcelli, G. Memory-effect based deconvolution microscopy for super-resolution imaging through scattering media. Sci. Rep. 6, 33558, (2016).

8. R. C. Gonzalez, and R. E. Woods, *Digital Image Processing*. (Pearson Education, 2011).
9. E. Y. Lam, and J. W. Goodman, "Iterative statistical approach to blind image deconvolution," Journal of the Optical Society of America A **17**, 1177-1184 (2000).
10. J. B. Sibarita, "Deconvolution microscopy," Advances in biochemical engineering, biotechnology, **95**, 201-243(2005).
11. D. S. C. Biggs, and M. Andrews, "Acceleration of iterative image estoration algorithms," Applied Optics **36**, 1766-1775 (1997).
12. L. B. Lucy, "An iterative technique for the rectification of observed distributions," The astronomical journal **79**, 745 (1974).
13. W. H. Richardson, "Bayesian-Based Iterative Method of Image Restoration," Journal of the Optical Society of America A **62**, 55-59 (1972).
14. J. Gurland, and R. C. Tripathi, "A Simple Approximation for Unbiased Estimation of the Standard Deviation, " The American Statistician **25**, 30-32 (1971).